Journal of Cleaner Production 229 (2019) 695–705

Contents lists available at ScienceDirect

Journal of Cleaner Production

journal homepage: www.elsevier.com/locate/jclepro

Impact analysis of carbon prices on metal mining projects by block-based estimation model: Implications for cleaner production

Yang Liu [a, b, c, *], Fengyu Ren [a], Hangxing Ding [a]

[a] School of Resources and Civil Engineering, Northeastern University, Shenyang, Liaoning, 110819, China
[b] Department of Mining and Minerals Engineering, Virginia Tech, Blacksburg, VA, 24061, USA
[c] Beijing General Research Institute of Mining and Metallurgy, Beijing, 100160, China

ARTICLE INFO

Article history:
Received 14 October 2018
Received in revised form
30 April 2019
Accepted 5 May 2019
Available online 6 May 2019

Keywords:
Carbon dioxide emissions
Carbon price
Carbon intensity
Life cycle assessment
Metal mining industry

ABSTRACT

Carbon dioxide emissions pricing is employed as an approach to mitigate climate change. To analyze the impact of carbon prices on the metal mining industry, this paper presents a new block-based carbon dioxide emissions estimation model to assess the carbon dioxide emissions and carbon intensity in varying carbon prices, by employing the engineering-based inputs from life cycle of mineral production. Such engineering-based data of an iron case is provided to test the impact of carbon prices on mining projects. The results indicate that the negative impact of carbon prices on the profit of mining projects is more sensitive in low minerals prices, especially for underground method. On the other hand, carbon price rising facilitates the mitigation of carbon dioxide emissions, by lowering the ratio of excavated waste rocks to mined-out raw ore, which varies linearly with the emissions. The carbon dioxide emissions in the studied case decrease from 39.92 kg carbon dioxide eq per ton to 21.50 kg carbon dioxide eq per ton, and from 51.02 kg carbon dioxide eq per ton to 42.80 kg carbon dioxide eq per ton, for surface and underground method, respectively. The results of carbon intensity show that it keeps increasing due to carbon price rising, until the mining boundaries are optimized based on the increased carbon price.

1. Introduction

Carbon dioxide (CO_2) is the largest contributor to recent climate change (EPA, 2016). The metal mining industry plays an important role in global CO_2 emissions due to the increasing demand for metallic minerals (Liu, 2015; Qi et al., 2017). To achieve the goal of CO_2 emissions reduction, charges on CO_2 emissions, including carbon taxes and CO_2 emissions permit trading, are employed as an effective mitigation approach for CO_2 emissions (Pezzey and Jotzo, 2013; Lemoine and Traeger, 2016). CO_2 emissions' charges facilitate the movement from energy-intensive activities to the improvement of energy consumption efficiency (Wang and Lin, 2017), but its negative impact on economics has recently been reported (Wang et al., 2015; Moreno and da Silva, 2016). It is necessary to analyze the impact of carbon prices on the profit, CO_2 emissions, and carbon intensity of metal mining projects, for reasonable carbon pricing. However, such analysis is still restricted due to the absence of either sufficient detailed inventory or valid CO_2 emissions estimation model for individual projects. Therefore, based on the life cycle assessment (LCA) method (ISO 14040, 2006), this paper proposes a new block-based CO_2 emissions estimation model to fill this research gap, employing engineering-based data from current major mining pathways of open-pit and underground methods.

Different models have been developed for CO_2 emissions estimations in mining industry. One of the most commonly cited models provided by the Intergovernmental Panel on Climate Change (IPCC, 2006) is valid to estimate the CO_2 emissions in cement, lime and glass production. In addition to the model introduced by the IPCC, Ju et al. (2016) proposed a new methodology to estimate fugitive methane emissions from coal mining based on the analysis of gas geology, and gas emission features.

* Corresponding author. School of Resources and Civil Engineering, Northeastern University, Shenyang, Liaoning, 110819, China.
E-mail address: liuyoung711@gmail.com (Y. Liu).

https://doi.org/10.1016/j.jclepro.2019.05.052
0959-6526/

Norgate and Haque (2010) conducted a LCA for the mining and mineral processing of iron ore, bauxite and copper concentrates in Australia. Mudd (2010) provided the historical trends of greenhouse gases (GHG) emissions for gold and uranium production in Australia. Shao et al. (2016) employed a novel index decomposition method to uncover the driving factors of energy-related CO_2 emissions changes in China's mining sector and its five subsectors over the period of 1999–2013. Recent studies emphasized the calculation of CO_2 emissions and carbon intensity for national or regional mining sectors based on macro-scale economic data or public statistics. However, it is intractable to analyze the impact of carbon prices on the profit, CO_2 emissions, and carbon intensity for individual projects based on these production results (i.e., economic data or public statistics), because the variation of carbon prices will change the mining cost, as well as the mining boundary and associated outcomes (i.e., profit, CO_2 emissions, and carbon intensity). This means that the impact analysis of carbon prices on mining projects should involve carbon prices in the mining boundary determination process.

In the mining boundary determination process, the deposit and surrounding rocks are separated into blocks, and the profit or cost for dealing with the materials in each block can be calculated from the block's attributes, such as minerals price, degree of mineralization, location, and mining cost (Chatterjee et al., 2016; Epstein et al., 2012; Mai et al., 2018). Such evaluated blocks enable the employment of algorithms to determine the mining boundary (Lerchs and Grossman, 1965; O'Sullivan and Newman, 2015; Liu and Kozan, 2016). If the CO_2 emissions for dealing with the materials in each block are provided, the cost for CO_2 emitting in varying carbon prices can be taken into account as an attribute to update these evaluated blocks. The new mining boundary based on these reevaluated blocks is valid to analyze the impact of carbon prices on project's profit, CO_2 emissions, and carbon intensity. This paper therefore introduces a new model to estimate the CO_2 emissions of individual blocks from mining and mineral processing.

The rest of this paper is organized as follows. Section 2 introduces the block-based estimation model, including system boundaries and the correlations to obtain CO_2 emissions of individual blocks from engineering-based inputs in different mining and mineral processing stages. In Section 3, a case study is introduced to analyze the impact of varying carbon prices on the profit, CO_2 emissions, and carbon intensity of metal mining projects. Finally, the conclusion and contribution are discussed in Section 4.

2. Block-based CO_2 emission estimation modeling

2.1. System boundary definition

The extraction of metallic minerals involves open-pit and underground methods. The open-pit method (i.e., the surface method) is employed when the deposits of commercially viable minerals are embedded at shallow depths (Whittle et al., 2018). Wherever minerals occur as strands below rivers and hard rocks, or are uneconomically to be extracted by open-pit method, underground methods are preferable for the valuable mineral deposits (King et al., 2017). The system boundaries of life cycle of mineral production are provided in Fig. 1 by dividing deposit mining and processing into 8 stages: ventilation, drilling, blasting, loading, transportation, crushing and grinding, mineral processing, and reclamation.

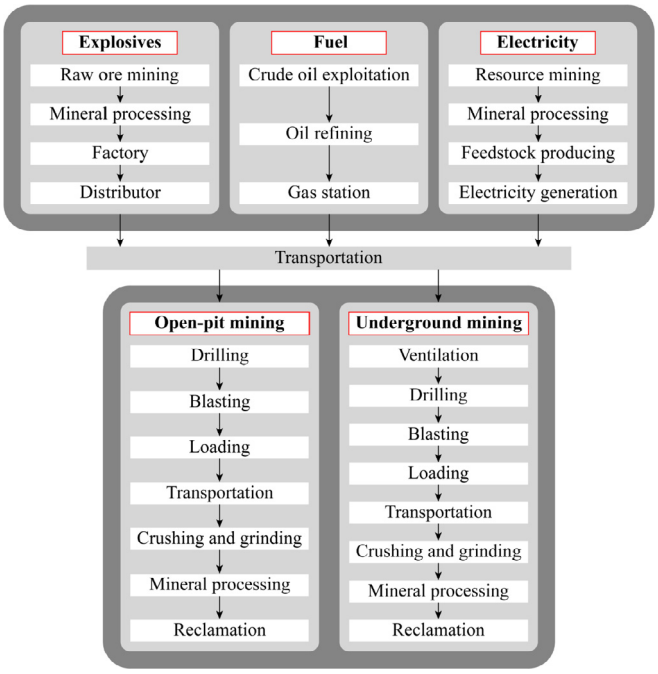

Fig. 1. System boundaries lifecycle of metal mining projects.

It should be noted that some limitations exist due to the system boundaries (Fig. 1). The proposed model is only valid for the metal mining projects with conventional methods consisted of the pathways illustrated in Fig. 1, i.e., open-pit method, and underground methods based on open-stope, caving and filling methods. The CO_2 emissions from the projects with other methods, e.g. leaching-based method (Farjana et al., 2018; Liu et al., 2018), cannot be calculated by this model.

2.2. CO_2 emissions estimation model

Each stage in the life cycle of mineral production is introduced in the follows.

2.2.1. Ventilation

Ventilation is employed in underground mines to maintain a favorable underground environment, which is required for breathing, thermal comfort and dispersal of harmful gases and dust (Akhtar et al., 2017). The mining industry uses fan systems for ventilation (Mayala et al., 2016), and the CO_2 emissions can be obtained by:

$$E_1^{un} = \frac{EF_{electricity} \cdot L^3 \cdot \rho \cdot P_1 \cdot 365 \cdot 24}{Q^{un}} \quad (1)$$

where E_1^{un} is the CO_2 emissions in the ventilation stage in t CO_2 eq; $EF_{electricity}$ is the emission factor of electricity in t CO_2 eq/kWh; L is the side length of a block in m; ρ is the average weight of materials in the block in ton/m^3; P_1 is the power of the underground ventilation fan system in kW; and Q^{un} is the annual production capacity of the underground project in ton/y.

2.2.2. Drilling

Drilling is an act of making blasting holes for explosives in both surface and underground mining projects (Kahraman et al., 2000).

In surface mining, the total length of blasting holes in a block is determined by the bench height, length and number of blasting holes (Shi et al., 2012). In underground mining, the total length of blasting holes in a block can be calculated according to the quantity of rock mass exploded by unit length of blasting hole, which varies with the property of rock mass (Brady and Brown, 2004). Eqs. (2a)–(2b) are employed to estimate the CO_2 emissions in surface and underground drilling, respectively:

$$E_2^{op} = \frac{EF_{fuel} \cdot \alpha \cdot P_2^{op} \cdot l \cdot L^3}{\eta_2^{op} \cdot s_2^{op} \cdot l' \cdot l'' \cdot h_b} \tag{2a}$$

$$E_2^{un} = \frac{EF_{electricity} \cdot L^3 \cdot \rho \cdot P_2^{un}}{\xi \cdot \eta_2^{un} \cdot s_2^{un}} \tag{2b}$$

where E_2^{op} and E_2^{un} are the CO_2 emissions from open-pit and underground drilling in t CO_2 eq; EF_{fuel} is the emission factor of fossil fuels, in t CO_2 eq/ton; α is the conversion coefficient from fossil fuel to electricity in mining equipment engines in ton/kWh; P_2^{op} and P_2^{un} are the power of surface and underground drills in kW; l is the length of a single surface blasting hole in m; η_2^{op} and η_2^{un} are the time utilization coefficients of surface and underground drills in %; s_2^{op} and s_2^{un} are the drilling speed of surface and underground drills in m/h; l' is the distance between adjacent rows of surface blasting holes in m; l'' is the distance between adjacent surface blasting holes in the same row in m; h_b is the height of the open pit bench in m; and ξ is the quantity of rocks exploded by unit length of underground blasting holes in ton/m.

2.2.3. Blasting

Blasting breaks intact rocks with the energy released from industrial explosives. A reasonable blasting design facilitates the stability of the open-pit slope (Shi and Chen, 2011), as well as the reduction of the ratio of oversized broken rocks (Shi et al., 2016). The CO_2 emissions in the blasting stage come from the consumption of industrial explosives, and can be calculated with:

$$E_3^{op} = \frac{EF_{explosive} \cdot L^3 \cdot q_{ex}^{op}}{1000} \tag{3a}$$

$$E_3^{un} = \frac{EF_{explosive} \cdot L^3 \cdot q_{ex}^{un}}{1000} \tag{3b}$$

where E_3^{op} and E_3^{un} are the CO_2 emissions from open-pit and underground blasting in t CO_2 eq; $EF_{explosive}$ is the emission factor of industrial explosives in t CO_2 eq/ton; q_{ex}^{op} and q_{ex}^{un} are the quantity of explosives consumed for breaking unit volume rocks in kg/m^3; and the value of q_{ex}^{op} and q_{ex}^{un} varies with the Protodyakonov coefficient of rock mass f (Xiao et al., 2015).

2.2.4. Loading

In surface projects, electric rope shovels, hydraulic mining shovels or excavators are available to collect and load the broken rocks into the transportation equipment at working face (Dunbabin and Corke, 2006; Tyulenev et al., 2017; Zheng et al., 2015). In some underground projects, scrapers can be utilized to collect and load the broken rocks into the branch entrances of draw shafts on each excavating level (Chi et al., 2012). But the scrapers sometimes are not necessary due to employment of load-haul-dump (LHD), which integrates collecting and transportation together (Dindarloo, 2016). The CO_2 emissions from LHDs will be discussed in transportation stage. Between different transportation equipment, the broken rocks are loaded via vibratory feeders (Czubak, 2012), e.g. at the exit of the draw shaft, or in the ore transfer station on surface. Eqs. (4a)–(4b) are provided to estimate the CO_2 emissions in surface and underground loading, respectively:

$$E_4^{op} = \frac{EF_{fuel} \cdot \alpha \cdot P_4^{op} \cdot k \cdot L^3 \cdot t_4^{op}}{\eta_4^{op} \cdot k_4^{op} \cdot V_4^{op} \cdot 3600} + \frac{EF_{electricity} \cdot P_{vf} \cdot L^3 \cdot \rho \cdot n_4^{op}}{Q_{vf}} \tag{4a}$$

$$E_4^{un} = \frac{EF_{electricity} \cdot P_4^{un} \cdot k \cdot L^3 \cdot t_4^{un}}{V_4^{un} \cdot 3600} + \frac{EF_{electricity} \cdot P_{vf} \cdot L^3 \cdot \rho \cdot n_4^{un}}{Q_{vf}} \tag{4b}$$

where E_4^{op} and E_4^{un} are the CO_2 emissions from surface and underground loading in t CO_2 eq; P_{vf}, P_4^{op}, P_4^{un} are the power of vibratory feeders, surface and underground loading equipment at working face in kW; k is the volumetric expansion coefficient of rocks in %; t_4^{op} and t_4^{un} are the operation time of surface and underground loading equipment at working face in a single loading cycle in second; η_4^{op} is the time utilization coefficient of surface loading equipment at working face in %; k_4^{op} is the charging ratio of surface loading equipment at working face in %; V_4^{op} and V_4^{un} are the standard capacities of surface and underground loading equipment at working face in single operating cycle in m^3; n_4^{op} and n_4^{un} are the times utilizing vibratory feeders between different transportation equipment in surface and underground mining in times; and Q_{vf} is the quantity of ore loaded via a vibratory feeder in unit time in ton/h.

2.2.5. Transportation

Off-road trucks, belt conveyors, and trains are employed in open-pit transportation individually or jointly (Erkayaoglu and Demirel, 2016). Belt conveyors have the largest transportation capacity but require uniform ore block size and good maintenance (Gladysiewicz et al., 2016). Off-road trucks, powered by diesel engines, are preferable to the other two due to the advantages of flexibility and reliability (Rodovalho and de Tomi, 2017). Underground transportation systems can be divided into the 4 subsystems of working face transportation, underground primary transportation, underground-to-surface hoisting, and surface transportation. In working face areas, LHDs are employed to collect and transport broken rocks from working face to the entrance of draw shaft. On the primary transportation level, the broken rocks are transported from draw shaft to hoisting shaft by underground trucks (Peterson, 2018), or tramcars hauled by electric locomotives (Jiang et al., 2017). Via shafts, the broken rocks are hoisted to the surface by cages or skip buckets (Lukichev et al., 2015). Finally, the broken rocks are transported to milling plants or waste dumps by surface transportation systems. The CO_2 emissions in surface and underground transportation can be obtained by:

$$E_5^{op} = \frac{EF_{fuel} \cdot \alpha \cdot P_t \cdot 2\,(\,\beta \cdot L_s + h_t\,) \cdot L^3 \cdot \rho}{\beta \cdot \eta_t \cdot v_t \cdot k_t \cdot Q_t} + \frac{EF_{electricity} \cdot P_{st} \cdot L^3 \cdot \rho \cdot 2 \cdot L_{st}}{v_{st} \cdot k_{st} \cdot Q_{st}} + \frac{EF_{electricity} \cdot P_{bc} \cdot L^3 \cdot \rho}{Q_{bc}} \tag{5a}$$

$$E_5^{un} = EF_{electricity}\left(\frac{k\cdot L^3\cdot 2\cdot\left(L_{LDH}+L_{LDH}^{'}\right)\cdot P_{LHD}}{\eta_{LDH}\cdot v_{LDH}\cdot k_{LDH}\cdot V_{LDH}}+\frac{k\cdot L^3\cdot 2\cdot L_{upt}\cdot P_{upt}}{\eta_{upt}\cdot v_{upt}\cdot k_{upt}\cdot V_{upt}}+\frac{L^3\cdot\rho\cdot P_h}{t_h\cdot k_h\cdot Q_h}\right) + \frac{EF_{fuel}\cdot\alpha\cdot P_t\cdot 2L_s^{un}\cdot L^3\cdot\rho}{\eta_t\cdot v_t\cdot k_t\cdot Q_t}+\frac{EF_{electricity}\cdot P_{st}\cdot L^3\cdot\rho\cdot 2\cdot L_{st}}{v_{st}\cdot k_{st}\cdot Q_{st}}+\frac{EF_{electricity}\cdot P_{bc}\cdot L^3\cdot\rho}{Q_{bc}} \quad (5b)$$

where E_5^{op} and E_5^{un} are the CO_2 emissions from surface and underground transportation in t CO_2 eq; P_t, P_{st}, P_{bc}, P_{LHD}, P_{upt}, and P_h are the power of off-road trucks, surface trains, belt conveyors, underground LHDs, transportation equipment on underground primary transportation level, and hoisters for cages or skip buckets in kW; β is the climbing ratio of open-pit roads in m/km; h_t is the vertical distance from the block bottom to open pit rim in m; L_s is the distance from open-pit rim to the destination of transported materials (e.g., ore transfer stations, milling plants or waste dumps) in km; L_{st}, L_{LDH} and $L_{LDH}^{'}$ are the haul distance of surface trains, and LHDs in sublevel tunnel and in sublevel access in km; L_{upt} is haul distance on primary transportation level in km; L_s^{un} is the distance from shaft exist on surface to destination of transported materials in km; η_t, η_{LDH}, and η_{upt} are the time utilization coefficient of off-road trucks, underground LHDs, and transportation equipment on underground primary transportation level in %; v_t, v_{st}, v_{LDH} and v_{upt} are the average speeds of off-road trucks, surface trains, underground LHDs and transportation equipment on underground primary transportation level in km/h; k_t, k_{st}, k_{LDH}, k_{upt}, and k_h are the charging ratios of off-road trucks, surface trains, underground LHDs, transportation equipment on underground primary transportation level, and hoisting equipment (i.e., cage or skip bucket) in %; Q_t, Q_{st}, and Q_h are the transportation capacities of an off-road truck, a surface train, and the hoisting equipment in a single cycle in ton; Q_{bc} is the transportation capacity of a belt conveyor in unit time in ton/h; V_{LDH} and V_{upt} are the standard bucket capacities of LDHs and transportation equipment on underground primary transportation level in m^3; and t_h is operating times of hoisting equipment in a hour in times/h.

2.2.6. Crushing and grinding

Crushing and grinding are required due to block-size requirements of the equipment for transportation and mineral processing (Rincon et al., 2019). According to the product size, this stage can be divided into preliminary crushing (under 250 mm), fine crushing (under 3 mm), and grinding (under 0.1 mm). The CO_2 emissions in this stage can be estimated by:

$$E_6^{op} = E_6^{un} = EF_{electricity}\left(\frac{L^3\cdot\rho\cdot P_{pc}}{\eta_{pc}\cdot Q_{pc}}+\frac{L^3\cdot\rho\cdot P_{fc}}{\eta_{fc}\cdot Q_{fc}}+\frac{L^3\cdot\rho\cdot P_g}{\eta_g\cdot Q_g}\right) \quad (6)$$

where E_6^{op} and E_6^{un} are the CO_2 emissions in surface and underground crushing and grinding in t CO_2 eq; P_{pc}, P_{fc} and P_g are the power of the equipment for preliminary crushing, fine crushing and grinding in kW; η_{pc}, η_{fc} and η_g are the time utilization coefficient of preliminary crushing, fine crushing and grinding equipment in %; and Q_{pc}, Q_{fc} and Q_g are the production capacities of preliminary crushing, fine crushing and grinding equipment in ton/h.

2.2.7. Mineral processing

The broken rocks mined out are separated into minerals and waste rocks by gravity, magnetic, flotation, or chemical concentration methods (Jordens et al., 2013). The CO_2 emissions in the mineral processing can be obtained by:

$$E_7^{op} = E_7^{un} = \frac{EF_{electricity}\cdot L^3\cdot\rho\cdot P_7}{\eta_7\cdot Q_7} \quad (7)$$

where E_7^{op} and E_7^{un} are the CO_2 emissions from processing the mined-out raw ore by surface and underground methods in t CO_2 eq; P_7 is the power of mineral processing equipment in kW; η_7 is the time utilization coefficient of mineral processing equipment in %; and Q_7 is the processing capacity of mineral processing equipment in ton/h.

2.2.8. Reclamation

Cleaner production targets for pollution prevention and environmental damage reduction in the life cycle of products (Dong et al., 2019). Due to the risk of pollution and ecological damage (Paricheh and Osanloo, 2017), reclamation is required after mining to eliminate surface damage, as well as to restore soil fertility for cultivating vegetation to natural conditions (Roy et al., 2016). Five key steps are involved in reclamation: land reconstruction including backfilling the mines with filling materials (e.g., waste rock and tailings; Villain et al., 2013; Lu et al., 2018), and dressing the surface with soil forming materials (e.g., loess; Li et al., 2013); amelioration of soil toxicity; irrigation engineering; biological restoration; and agro-ecosystem management (Miao and Marrs, 2000). Apart from the land reconstruction, it is intractable to estimate the CO_2 emissions of the other four steps in a changing environment, because of the involvement of chemistry, biology, and ecology (Milly et al., 2008). Therefore, this paper presents an equation to calculate CO_2 emissions only for land reconstruction. To recover the damage on surface due to mining, every mined-out block by open-pit method needs to be filled or dressed. On the other hand, due to the support from ore pillars or caved overburdened materials (Woo et al., 2013; Sui et al., 2015), whether an underground mined-out block requires land reconstruction has to be determined by empirical or analytical prediction models, such as Laubscher (1994), Hoek (1974), and Sepehri et al. (2017). If a block needs to be reconstructed, the following equation is valid to estimate the CO_2 emissions:

$$E_8^{op} = E_8^{un} = EF_{fuel}\cdot\alpha\cdot\left(\frac{P_8\cdot L^3\cdot t_8}{\eta_8\cdot k_8\cdot V_8\cdot 3600}+\frac{P_t\cdot 2L_8\cdot L^3\cdot\rho^{'}}{\eta_t\cdot v_t\cdot k_t\cdot Q_t}\right) \quad (8)$$

where E_8^{op} and E_8^{un} are the CO_2 emissions from land reconstruction in open-pit and underground mining in t CO_2 eq; P_8 is the power of the loading equipment at where the land reconstruction materials are collected in kW; t_8 is the operation time of loading equipment for land reconstruction in a loading cycle in second; η_8 is the time utilization coefficient of loading equipment for land reconstruction in %; k_8 is the charging ratio of loading equipment for land reconstruction in %; V_8 is the standard capacity of loading equipment for land reconstruction in m^3; $\rho^{'}$ is the average weight of backfilling

materials in ton/m^3; L_8 is the distance from land reconstruction area to the place where backfilling materials are collected in km.

Eqs. (1)–(8) list the engineering-based inputs required to calculate the CO_2 emissions from mining and processing the materials in a block. If these inputs are provided, the CO_2 emissions for dealing with the materials in a block can be calculated by substituting the results from Eqs. (1)–(8) into:

$$E_n^i = \sum_{j=1}^{j_\cdot} E_{n,j}^i \tag{9}$$

where E_n^i is the CO_2 emissions from mining and processing the materials in block n by method i in t CO_2 eq; i represents the mining methods of the project, i = op, open-pit method, i = un, underground method; n is the sequential number of blocks; $E_{n,j}^i$ is the CO_2 emissions in stage j for dealing with the materials in block n by method i in t CO_2 eq; $j_\cdot$ represents the stages required by the block n; $j_\cdot$ is determined by the utilized mining method and the degree of mineralization obtained from geo-statistics (Paithankar and Chatterjee, 2018). For instance, if a project uses block-caving method to excavate the deposit, neither drilling nor blasting is required for mining and processing the material in blocks (Rafiee et al., 2018). Mineral processing is not required for all the blocks with waste rocks as well. Additionally, the equipment listed in Eqs. (1)–(8) is optional in some cases. If this occurs, the power of the unemployed equipment equals to 0. For instance, if all the excavated materials are transported by off-road trucks for an open-pit project, the power of the other equipment in the transportation stage is 0 (i.e., $P_{st} = 0$, $P_{bc} = 0$, in Eq. (5a)).

The results of CO_2 emissions from mining and processing the material in each block enable the consideration of CO_2 emitting cost in the determination of mining boundary. If the mining boundary is provided, the CO_2 emissions and carbon intensity of a project can be obtained by:

$$EF^i = \frac{\sum_{n=1}^{n_\cdot}\sum_{j=1}^{j_\cdot} E_{n,j}^i}{Q_{total}^i} \tag{10}$$

$$CI^i = \frac{\sum_{n=1}^{n_\cdot}\sum_{j=1} E_{n,j}^i}{NPV^i} \tag{11}$$

where EF^i is the CO_2 emissions of the project in kg CO_2 eq per ton; $n_\cdot$ represents the number of blocks in the mining boundary; Q_{total}^i is the quantity of minerals produced in the project by method i in k ton; CI^i is the carbon intensity of the project by method i in t CO_2 eq per k dollars; and NPV^i is the net present value (NPV) of the project by method i in k dollars.

The contribution of each operation to the CO_2 emissions can be estimated by:

$$EF_j^i = \sum_{n=1}^{n_\cdot} E_{n,j}^i \tag{12}$$

where EF_j^i is the CO_2 emissions of the project in stage j in kg CO_2 eq per ton.

The employment of the engineering-based inputs enables the proposed model to provide detailed CO_2 emissions from different operations. There are two models closely linked to this model due to the involvement of engineering-based inputs. One of them is the Oil Production Greenhouse Gas Emissions Estimator (OPGEE; El-Houjeiri et al., 2017), which can estimate the GHG emissions during the 7 stages of crude petroleum production. Based on OPGEE v2.0a and intensive well-to-refinery data from 146 oilfields in 20 countries, Masnadi et al. (2018) analyzed the contributions of each oil production stage to the CO_2 emissions of China's oil supply. The other one is the GreenHouse gas emissions of current Oil Sands Technologies (GHOST), which can provide GHG emissions in oil sands production, based on actual operating and process performance data from industry (Charpentier et al., 2011; Sleep et al., 2018). Compared with both OPGEE and GHOST, the employment of block model enables the proposed model to be applicable in mining boundary design or optimization. This means this model has the potential to mitigate the CO_2 emissions of metal mining projects before implementation.

On the other hand, some limitations of the proposed model due to the block model should be addressed. This model is only valid to obtain the CO_2 emissions from the operations that can be calculated in each block individually, as listed in Fig. 1. But the CO_2 emissions from other operations, such as dewatering, lighting, and road construction, cannot be estimated by this model, because they are not directly related to the excavation of a certain block.

3. Case study

To test the impact of carbon prices on projects' profit, CO_2 emissions, and carbon intensity, the case of Yanqianshan iron mine is introduced, which is currently in the transition from open-pit to underground mining (Xu et al., 2016). The contributions of different mining stages to the CO_2 emissions in varying carbon prices and minerals prices (i.e., Fe concentrates prices) are also tested.

3.1. Inventory analysis

The system boundaries (Fig. 1) reveal that the CO_2 emissions from mineral production come from the consumption of fossil fuels, industrial explosives and electricity. IPCC (2006) provided the default CO_2, CH_4 and N_2O emission factors of some fossil fuels. Based on higher heating values (HHV; Wang, 2010) and global warming potential (GWP; Stocker et al., 2013), the emission factors of fossil fuels are converted into t CO_2 eq per ton fossil fuel. Due to the significant effect of additives (e.g., wood, TNT) and environmental factors (e.g., temperature, pressure; Zhou et al., 2018) on the blasting reactions, it is intractable to obtain a definite equation to calculate the CO_2 emission factors of industrial explosives. This paper uses Brinkley-Wilson method to deduce the gaseous products from the composition of the explosives (Pepekin and Gubin, 2007). The emission factors (in t CO_2 eq per ton) of the explosives can be therefore calculated from these gaseous products, HHV and GWP. Electricity is an indirect emissions source, and its emission factor varies in different regions (Ogland-Hand et al., 2019). The National Development and Reform Commission (NDRC, 2016) provides the emission factor for the region, where the studied case locates. Table 1 lists the emission factors of the carbon sources in this study.

3.2. Block-based CO_2 emissions results

Since the project of Yanqianshan iron mine has been implemented for more than 50 years, it is intractable to estimate the CO_2 emissions with varying mining and mineral processing equipment. Based on its mining method and production capacity, the mining equipment is reselected with reference to similar projects, as shown in Table A1. Table A2 provides the engineering-based inputs from production details and equipment parameters. Such inputs and the map of mineralized zone provided by the studied project enable the proposed model to estimate the CO_2 emissions from mining and processing the materials in each block, which is illustrated in Fig. 2. Because underground mining uses sublevel caving

method, the quantity of materials for land reconstruction and dressing has to be determined based on the mining boundary designs (Woo et al., 2013). The results in Fig. 2(b) do not include the CO_2 emissions in the reclamation stage.

3.3. The impact of carbon prices on project's profit

To test the impact of carbon prices on project's profit, the mining boundaries are designed in varying carbon prices and minerals prices, based on the principle of NPV maximization (King et al., 2017). The CO_2 emissions from land reconstruction in underground mining are calculated in varying mining boundaries. Then, the cost for land reconstruction and associated CO_2 emitting is calculated to update the mining boundaries until the principle of NPV maximization is satisfied. Fig. 3 provides the distribution of the project's profit obtained by surface and underground methods.

It can be observed that the profit keeps decreasing with the increase of carbon prices at a constant minerals price, until the project becomes unprofitable (e.g., minerals price = 50 dollars per ton, carbon price = 150 dollars per ton CO_2 eq in surface mining; and minerals price = 50 dollars per ton, carbon price = 50, 75, 100, 125, and 150 dollars per ton CO_2 eq in underground mining). This negative impact of carbon prices on the projects' profit is also reported by Xu et al. (2014). The researchers conducted sensitivity analysis of the project's profit versus carbon prices in varying minerals prices, and the results are shown in Fig. 4.

The results of sensitivity analysis reveal that a negative correlation trend exists between the sensitivity of project's profit and minerals price for both surface and underground mining. On the other hand, at a constant minerals price, the profit by underground method presents a more noticeable variation than that by surface method. Such phenomena indicate that the impact of carbon prices on the profit of mining projects is more significant when minerals prices are low, especially for the projects by underground method.

3.4. The impact of carbon prices on CO_2 emissions

Fig. 5 provides the distribution of CO_2 emissions in varying carbon prices and minerals prices, in which the results with same value demonstrate that these cases have the same mining boundary design. It can be observed that the CO_2 emissions present decreasing trends (from 39.92 kg CO_2 eq per ton to 21.50 kg CO_2 eq per ton for open-pit method; from 51.02 kg CO_2 eq per ton to 42.80 kg CO_2 eq per ton for underground method), when the carbon price increases. Fig. 6 provides the relationship between CO_2 emissions and mining boundaries, which are represented by the ratio of excavated waste rocks to mined-out raw ore (i.e., the stripping ratio in open-pit mining; Rahmanpour and Osanloo, 2017). It can be observed that the CO_2 emissions strongly vary linearly ($R^2 > 0.99$) with the ratio of excavated waste rocks to mined-out raw ore for both surface and underground results, and the relationships can be expressed as follows:

$$EF^{op} = 10.375\, R^{op} + 12.489$$

$$EF^{un} = 45.995\, R^{un} + 7.7464 \quad (13)$$

where EF^{op} and EF^{un} are the CO_2 emissions from surface and underground mining in kg CO_2 eq per ton; and R^{op} and R^{un} are the ratio of excavated waste rocks to mined-out raw ore by the surface and underground methods.

Such linear relationships demonstrate that charging for CO_2

Table 1
CO_2 emission factors for mineral production.

Source		Emission factor
Fossil fuel	Gasoline	3.24404 t CO_2 eq/ton
	Diesel	3.39581 t CO_2 eq/ton
Explosives	No.2 granulated ammonium nitrate	0.22218 t CO_2 eq/ton
	Rock colloidal emulsion explosive	0.10109 t CO_2 eq/ton
Electricity	Northeastern China regional power grid	1.1171×10^{-3} t CO_2 eq/kWh

Note: Since Yanqianshan iron mine is located in Liaoning, China, the emission factors of electricity come from the northeastern China regional power grid (NDRC, 2016).

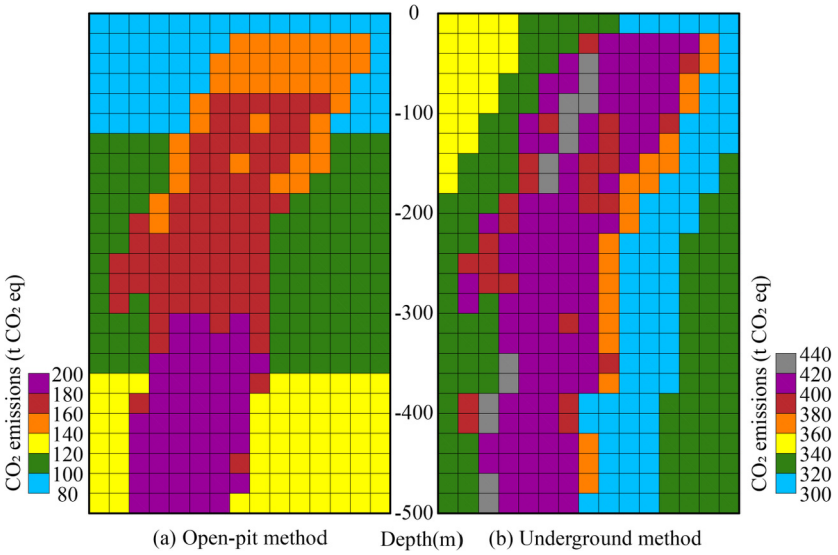

Fig. 2. Block-based CO_2 emissions results on a deposit's section. Note: The size of each block is 20 m × 20 m × 20 m.

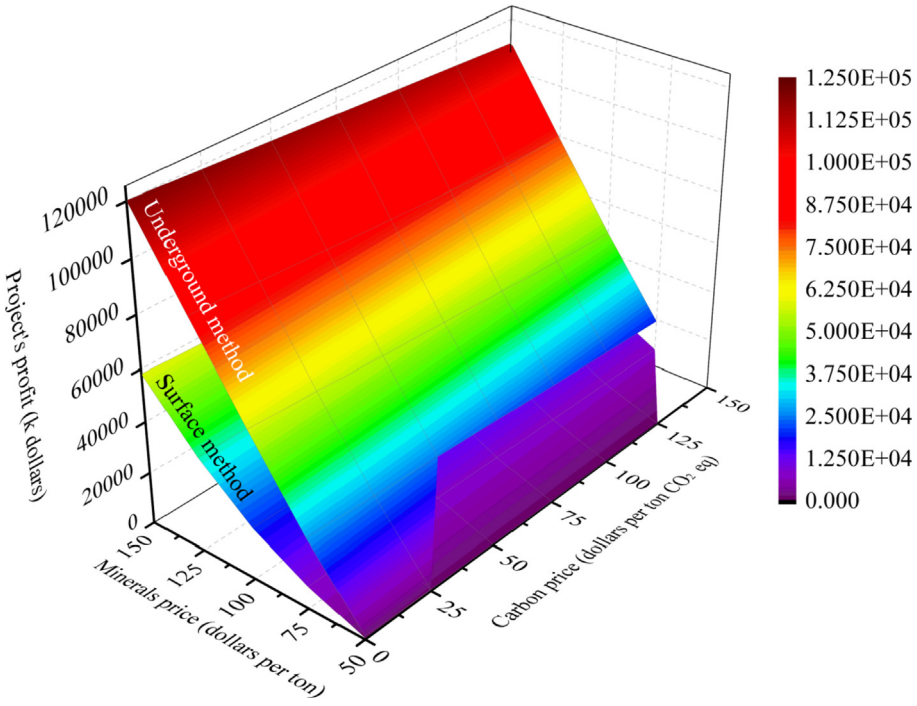

Fig. 3. Distribution of the profit in varying minerals and carbon prices.

emitting is an effective mitigation approach, and it works by changing the mining boundary. The contributions of mining and mineral processing operations to the CO_2 emissions (Fig. 6) account for this mitigation. Fig. 6(a) shows that the contributions of transportation (from 26.98% to 34.26%) and reclamation (from 27.01% to 29.66%) to the CO_2 emissions from surface mining increase with the growth of stripping ratio. Meanwhile, the contribution of crushing and grinding presents a significant reduction (from 25.42% to 14.52%), even though its CO_2 emissions increase from 5.47 kg CO_2 eq per ton to 5.82 kg CO_2 eq per ton. This phenomenon helps to uncover the reason for the increase of CO_2 emissions. When the stripping ratio increases, more waste rocks are excavated for producing unit mineral product. The CO_2 emissions increase because these additional excavated waste rocks require the same mining operations as mined-out raw ore, except for mineral processing, crushing and grinding. Same phenomenon is also observed in underground mining (Fig. 6(b)). Even though the CO_2 emissions of underground mining is dominated by transportation (more than 60%), the contribution of crushing and grinding decreases from 12.23% to 11.73% (meanwhile, its CO_2 emissions increase from 5.24 kg CO_2 eq per ton to 5.99 kg CO_2 eq per ton), due to the increase of the ratio of excavated waste rocks to mined-out raw ore. If the ratio is lowered, less waste rocks will be excavated for producing unit mineral product. The elimination of the CO_2 emissions for dealing with these additional waste rocks (i.e., drilling, blasting, and transportation) accounts for the mitigation of CO_2 emissions.

3.5. The impact of carbon prices on carbon intensity

Fig. 7 shows the distribution of carbon intensity in varying minerals prices and carbon prices. When the minerals prices are low (50 and 75 dollars per ton), the carbon intensity of underground method is much higher than that by the surface method. However, the carbon intensity of underground mining presents a

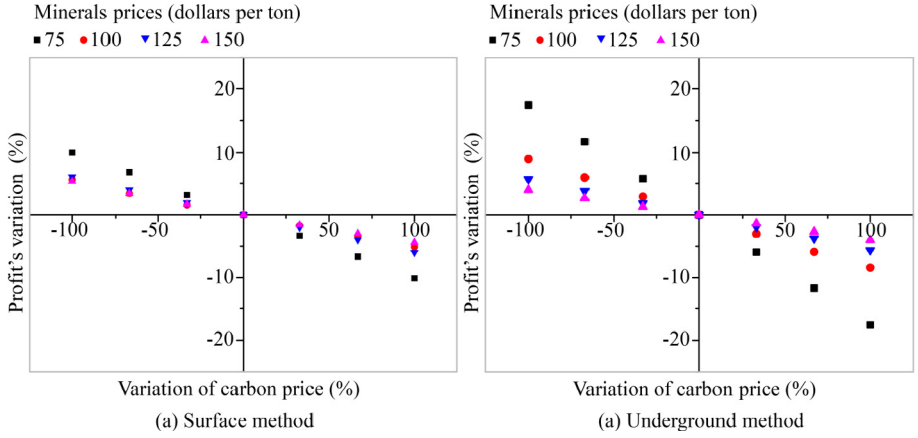

Fig. 4. Sensitivity analysis of the case's profit versus carbon price.

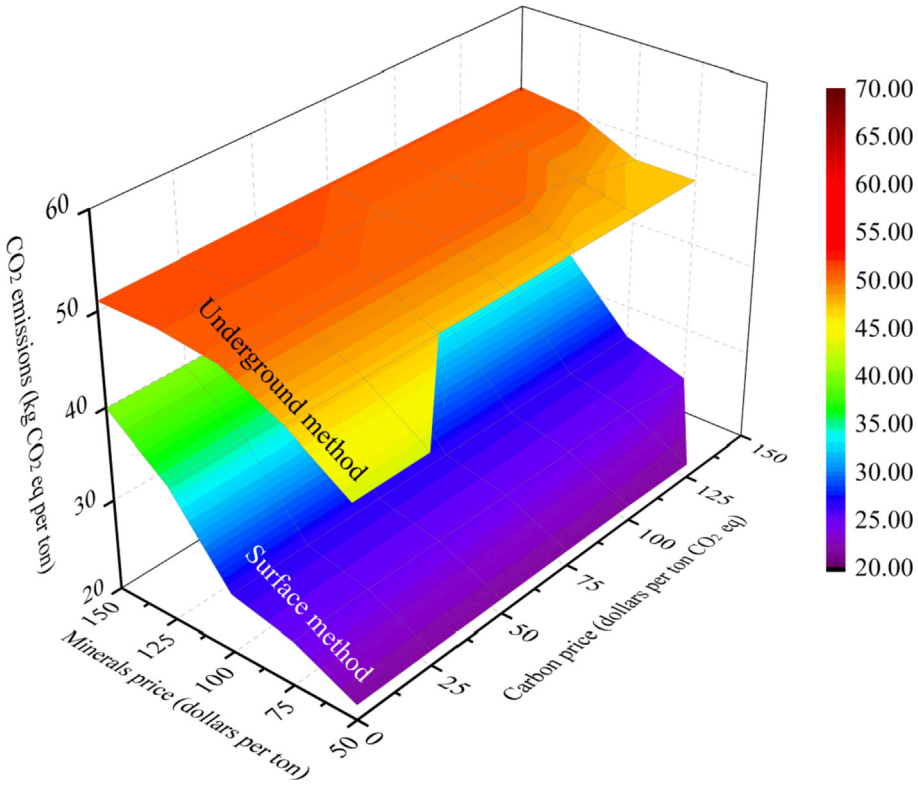

Fig. 5. Distribution of CO_2 emissions in varying minerals and carbon prices.

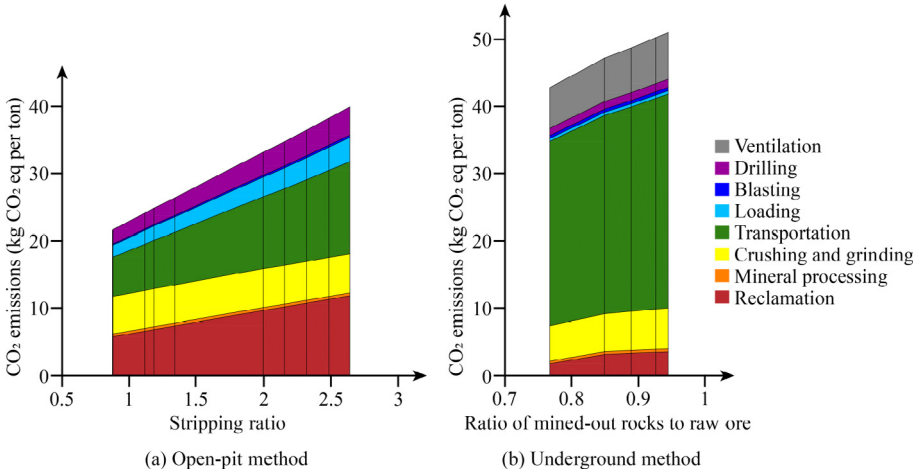

Fig. 6. Contributions of different mining stages to CO_2 emissions.

more significant decrease and falls below that by surface mining when the minerals price reaches 150 dollars per ton.

Fig. 7 also reveals that the impact of carbon prices on carbon intensity is positive, when mining boundary (i.e., the ratio of excavated waste rocks to mined-out raw ore) and minerals price are constant. For instance, when minerals price = 125 dollars per ton and $R^{op} = 2.150$, the carbon intensity by open-pit method increases from 0.752 t CO_2 eq per k dollars (carbon price = 0) to 0.783 t CO_2 eq per k dollars (carbon price = 50 dollars per ton CO_2 eq). However, sudden reduction of carbon intensity appears when the increase of carbon prices causes mining boundary shrinking (i.e., R^{op} decreasing). For instance, the carbon intensity decreases from 0.783 t CO_2 eq per k dollars (minerals price = 125 dollars per ton, carbon price = 50 dollars per ton CO_2 eq, $R^{op} = 2.150$) to 0.700 t CO_2 eq per k dollars (minerals price = 125 dollars per ton, carbon price = 75 dollars per ton CO_2 eq, $R^{op} = 1.995$). Same phenomenon is also observed in underground mining. Such phenomena indicate the carbon price rising contributes to carbon intensity reduction only when it reduces the ratio of excavated waste rocks to mined-out raw ore (i.e., mining boundary shrinking). However, because the mining boundary is a strategic decision (Liu and Kozan, 2016; Rahmanpour and Osanloo, 2017), the carbon price rising increases the carbon intensity of the projects in production, before they optimize the mining boundary based on the increased carbon price.

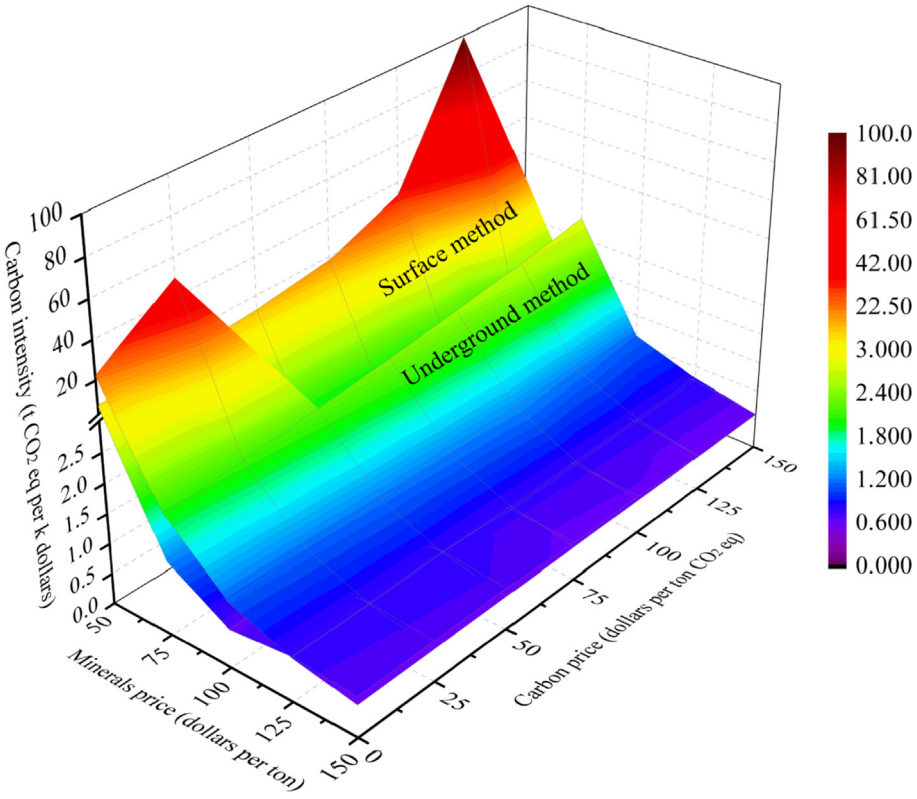

Fig. 7. Distribution of carbon intensity in varying minerals and carbon prices.

4. Conclusion

To analyze the impact of carbon prices on the profit, CO_2 emissions, and carbon intensity of metal mining projects, this paper introduces a new block-based CO_2 emissions estimation model, employing engineering-based data from mining and mineral processing operations. Such engineering-based data of a project regarding mining equipment and production details is provided, which is a contribution due to the absence of sufficient inventory in the literature.

The impact analysis of carbon prices on a case's profit, CO_2 emissions, and carbon intensity is conducted. The carbon prices have a negative impact on the case's profit, and this impact is more sensitive to low minerals prices, especially for the underground method. Carbon price increasing facilitates the mitigation of CO_2 emissions, which decrease from 39.92 kg CO_2 eq per ton to 21.50 kg CO_2 eq per ton, and from 51.02 kg CO_2 eq per ton to 42.80 kg CO_2 eq per ton for open-pit and underground method, respectively. The impact of carbon prices on CO_2 emissions works by changing the ratio of excavated waste rocks to mined-out raw ore, which linearly relates to CO_2 emissions of mining projects. On the other hand, the results of carbon intensity indicate the carbon price rising facilities carbon intensity reduction only when it causes mining boundary shrinking, otherwise, it leads to carbon intensity increase. For the projects in production, carbon price rising will increase the carbon intensity in a long duration of time, because the mining boundary design is strategic.

The contribution of this proposed model is in both theory and practice. It is valid not only to provide detailed engineering-based inventory theoretically, but also to guide mining companies to implement actions for CO_2 emissions mitigation or carbon intensity reduction in the initial design before the implementation of mining projects.

Acknowledgements

This work was supported by the National Natural Science Foundation of China [grant number 51534003]; the Ministry of Science and Technology of the People's Republic of China [grant number 2016YFC0801601]; and the China Scholarship Council [grant number 20160608056].

Appendix

Table A1
Mining and processing equipment involved in the Yanqianshan iron mine

Stage	Surface method	Underground method
Ventilation		K40-6-No.20
Drilling	CAT MD6250	Sandvik DL311
Blasting	No.2-rock-GAN	No.2-rock-GAN
Loading	CAT 6015B	FZC4/1.2 × 2–7.5
Transportation	CAT 777E	CAT R1700G (LDH) ZK40-9/550 (Electric locomotive) Citic IC JKM4.5 × 6 (Hoister) CAT 777E (Surface)
Preliminary crushing	Sandvik CJ815	Sandvik CJ815
Fine crushing	Citic IC PCX150	Citic IC PCX150
Mineral processing	Citic IC CTB1530	Citic IC CTB1530
Reclamation	CAT 6015B (loading) CAT 777E (transportation)	CAT 6015B (loading) CAT 777E (transportation)

Table A2
Engineering-based inputs from production details and equipment parameters

Notations	Parameters	Notations	Parameters
Q^{op}	3×10^6 ton/y	Q^{un}	8×10^6 ton/y
ρ	3.4 ton/m^3 (ore), 2.9 ton/m^3(waste rock)	k	1.5
α	0.206×10^{-3} ton/kWh (diesel engine)	L	20 m
P_1	160 kW × 12 (electricity)	P_2^{op}	655 kW(diesel engine)
P_2^{un}	75kw(electricity)	s_2^{op}	35 m/h
s_2^{un}	23 m/h	η_2^{op}	80%
η_2^{un}	80%	l	14 m
$l^{'}$	3.5 m	$l^{''}$	4 m
h_b	12 m	ξ	11 ton/m
q_{ex}^{op}	2.45 kg/m^3	q_{ex}^{un}	0.6 kg/m^3
P_4^{op}	606 kW (diesel)	t_4^{op}	30 s
η_4^{op}	60%	k_4^{op}	80%
V_4^{op}	8.1 m^3	P_{vf}	15 Kw (electricity)
Q_{vf}	1910 ton/h	n_4^{op}	0
n_4^{un}	1	P_t	758 kW (diesel engine)
β	50 m/km	L_s	7 km
η_t	80%	v_t	40 km/h
k_t	90%	Q_t	98 t
P_{LHD}	263kw (electricity)	L_{LDH}	0.2 km
η_{LDH}	60%	v_{LDH}	10 km/h
k_{LDH}	90%	V_{LDH}	5.7 m^3
L_{upt}	3 km	P_{upt}	440 kW (electricity)
η_{upt}	90%	v_{upt}	12 km/h
k_{upt}	95%	V_{upt}	10 m^3 × 16
P_h	5400 kW (electricity)	t_h	32 times/h
k_h	95%	Q_h	32 t
L_s^{un}	7 km	P_{pc}	200 kw (electricity)
η_{pc}	90%	Q_{pc}	676.8 ton/h
P_{fc}	200 kw (electricity)	η_{fc}	90%
Q_{fc}	150 ton/h	P_7	11 kw (electricity)
η_7	95%	Q_7	170 ton/h
L_8	7 km	$\rho^{'}$	2.71 ton/m^3

References

Akhtar, S., Kumral, M., Sasmito, A.P., 2017. Correlating variability of the leakage characteristics with the hydraulic performance of an auxiliary ventilation system. Build. Environ. 121, 200–214. https://doi.org/10.1016/j.buildenv.2017.05.029.

Brady, B.H.G., Brown, E.T., 2004. Rock Mechanics for Underground Mining, third ed. Springer, Dordrecht.

Charpentier, A.D., Kofoworola, O., Bergerson, J.A., MacLean, H.L., 2011. Life cycle greenhouse gas emissions of current oil sands technologies: GHOST model development and illustrative application. Environ. Sci. Technol. 45, 9393–9404. https://doi.org/10.1021/es103912m.

Chatterjee, S., Sethi, M.R., Asad, M.W.A., 2016. Production phase and ultimate pit limit design under commodity price uncertainty. Eur. J. Oper. Res. 248, 658–667. https://doi.org/10.1016/j.ejor.2015.07.012.

Chi, H.P., Zhan, K., Shi, B.Q., 2012. Automatic guidance of underground mining vehicles using laser sensors. Tunn. Undergr. Space Technol. 27, 142–148. https://doi.org/10.1016/j.tust.2011.08.007.

Czubak, P., 2012. Reduction of forces transmitted to the foundation by the conveyor or feeder operating on the basis of the frahm's eliminator, at a significant loading with feed. Arch. Min. Sci. 57, 1121–1136. https://doi.org/10.2478/v10267-012-0074-6.

Dindarloo, S., 2016. Reliability forecasting of a load-haul-dump machine: a comparative study of ARIMA and neural networks. Qual. Reliab. Eng. Int. 32, 1545–1552. https://doi.org/10.1002/qre.1844.

Dong, L., Tong, X., Li, X., Zhou, J., Wang, S., Liu, B., 2019. Some developments and new insights of environmental problems and deep mining strategy for cleaner production in mines. J. Clean. Prod. 210, 1562–1578. https://doi.org/10.1016/j.jclepro.2018.10.291.

Dunbabin, M., Corke, P., 2006. Autonomous excavation using a rope shovel. J. Field Robot. 23, 379–394. https://doi.org/10.1002/rob.20132.

El-Houjeiri, H.M., Masnadi, M.S., Vafi, K., Duffy, J., Brandt, A.R., 2017. Oil Production Greenhouse Gas Emissions Estimator OPGEEv2.0a: User Guide and Technical Documentation. https://pangea.stanford.edu/departments/ere/dropbox/EAO/OPGEE/OPGEE_documentation_v2.0a.pdf/. (Accessed 27 March 2017).

Environmental Protection Agency, 2016. Climate Change Indicators: Global Greenhouse Gas Emissions. https://www.epa.gov/climate-indicators/climate-change-indicators-global-greenhouse-gas-emissions/. (Accessed May 2014).

Epstein, R., Goic, M., Weintraub, A., Catalan, J., Santibanez, P., Urrutia, R., Cancino, R., Gaete, S., Aguayo, A., Caro, F., 2012. Optimizing long-term production plans in underground and open-pit copper mines. Oper. Res. 60, 4–17. https://doi.org/10.1287/opre.1110.1003.

Erkayaoglu, M., Demirel, N., 2016. A comparative life cycle assessment of material handling systems for sustainable mining. J. Environ. Manag. 174, 1–6. https://doi.org/10.1016/j.jenvman.2016.03.011.

Farjana, S.H., Huda, N., Mahmud, M.A.P., Lang, C., 2018. Comparative life-cycle assessment of uranium extraction processes. J. Clean. Prod. 202, 666–683. https://doi.org/10.1016/j.jclepro.2018.08.105.

Gladysiewicz, L., Kawalec, W., Krol, R., 2016. Selection of carry idlers spacing of belt conveyor taking into account random stream of transported bulk material. Eksploat. Niezawodn. 18, 32–37. https://doi.org/10.17531/ein.2016.1.5.

Hoek, E., 1974. Progressive caving induced by mining an inclined orebody. Trans. Inst. Min. Metall. 83, A133–A139.

Intergovernmental Panel on Climate Change, 2006. 2006 IPCC Guidelines for National Greenhouse Gas Inventories. Kanagawa, Japan.

International Organization for Standardization, 2006. Environmental Management - Life Cycle Assessment: Principles and Framework (ISO 14040). Geneva, Switzerland.

Jiang, Y., Li, Z.X., Yang, G., Zhang, Y.L., Zhang, X.G., 2017. Recent progress on smart mining in China: unmanned electric locomotive. Adv. Mech. Eng. 9, 1687814017695045. https://doi.org/10.1177/1687814017695045.

Jordens, A., Cheng, Y.P., Waters, K.E., 2013. A review of the beneficiation of rare earth element bearing minerals. Miner. Eng. 41, 97–114. https://doi.org/10.1016/j.mineng.2012.10.017.

Ju, Y.W., Sun, Y., Sa, Z.Y., Pan, J.N., Wang, J.L., Hou, Q.L., Li, Q.G., Yan, Z.F., Liu, J., 2016. A new approach to estimate fugitive methane emissions from coal mining in China. Sci. Total Environ. 543, 514–523. https://doi.org/10.1016/j.scitotenv.2015.11.024.

Kahraman, S., Balci, C., Yazici, S., Bilgin, N., 2000. Prediction of the penetration rate of rotary blast hole drills using a new drillability index. Int. J. Rock Mech. Min. 37, 729–743. https://doi.org/10.1016/S1365-1609(00)00007-1.

King, B., Goycoolea, M., Newman, A., 2017. Optimizing the open pit-to-underground mining transition. Eur. J. Oper. Res. 257, 297–309. https://doi.org/10.1016/j.ejor.2016.07.021.

Laubscher, D.H., 1994. Cave mining - the state of the art. J. S. Afr. Inst. Min. Metall 94, 279–293.

Lemoine, D., Traeger, C.P., 2016. Economics of tipping the climate dominoes. Nat. Clim. Change 6, 514–519. https://doi.org/10.1038/nclimate2902.

Lerchs, H., Grossman, I., 1965. Optimum design of open-pit mines. Can. Min. Metall. Bull. 58, 47–54.

Li, S.Q., Di, X.Y., Wu, D.M., Zhang, J.T., 2013. Effects of sewage sludge and nitrogen fertilizer on herbage growth and soil fertility improvement in restoration of the abandoned opencast mining areas in Shanxi, China. Environ. Earth Sci 70, 3323–3333. https://doi.org/10.1007/s12665-013-2397-9.

Liu, Z., 2015. China's carbon emissions report 2015. Sustainability science program and energy technology innovation policy research group. In: Belfer Center Discussion Paper #2015-02. Harvard Kennedy School of Government, Cambridge, MA.

Liu, S.Q., Kozan, E., 2016. New graph-based algorithms to efficiently solve large scale open pit mining optimisation problems. Expert Syst. Appl. 43, 59–65. https://doi.org/10.1016/j.eswa.2015.08.044.

Liu, J.H., Chen, L.K., Liu, C.Y., Qiu, L.R., He, S., 2018. Pb speciation in rare earth minerals and use of entropy and fuzzy clustering methods to assess the migration capacity of Pb during mining activities. Ecotoxicol. Environ. Saf. 165, 334–342. https://doi.org/10.1016/j.ecoenv.2018.09.007.

Lu, H.J., Qi, C.C., Chen, Q.S., Gan, D.Q., Xue, Z.L., Hu, Y.J., 2018. A new procedure for recycling waste tailings as cemented paste backfill to underground stopes and open pits. J. Clean. Prod. 188, 601–612. https://doi.org/10.1016/j.jclepro.2018.04.041.

Lukichev, S.V., Belogorodtsev, O.V., Gromov, E.V., 2015. Justification of methods to open up ore bodies with various combinations of conveyor transport. J. Min. Sci. 51, 513–521. https://doi.org/10.1134/S1062739115030126.

Mai, N.L., Topal, E., Erten, O., 2018. A new open-pit mine planning optimization method using block aggregation and integer programming. J. S. Afr. Inst. Min. Metall 118, 705–714. https://doi.org/10.17159/2411-9717/2018/v118n7a4.

Masnadi, M.S., El-Houjeiri, H.M., Schunack, D., Li, Y.P., Roberts, S.O., Przesmitzki, S., Brandt, A.R., Wang, M., 2018. Well-to-refinery emissions and net-energy analysis of China's crude-oil supply. Nat. Energy 3, 220–226. https://doi.org/10.1038/s41560-018-0090-7.

Mayala, L.P., Veiga, M.M., Khorzoughi, M.B., 2016. Assessment of mine ventilation systems and air pollution impacts on artisanal tanzanite miners at M-erelani, Tanzania. J. Clean. Prod. 116, 118–124. https://doi.org/10.1016/j.jclepro.2016.01.002.

Miao, Z., Marrs, R., 2000. Ecological restoration and land reclamation in open-cast mines in Shanxi Province, China. J. Environ. Manag. 59, 205–215. https://doi.org/10.1006/jema.2000.0353.

Milly, P.C.D., Betancourt, J., Falkenmark, M., Hirsch, R.M., Kundzewicz, Z.W., Lettenmaier, D.P., Stouffer, R.J., 2008. Stationarity is dead: whither water management? Science 319, 573–574. https://doi.org/10.1126/science.1151915.

Moreno, B., da Silva, P.P., 2016. How do Spanish polluting sectors' stock market returns react to European Union allowances prices? A panel data approach. Energy 103, 240–250. https://doi.org/10.1016/j.energy.2016.02.094.

Mudd, G.M., 2010. The Environmental sustainability of mining in Australia: key mega-trends and looming constraints. Resour. Pol. 35, 98–115. https://doi.org/10.1016/j.resourpol.2009.12.001.

National Development, Reform Commission, 2016. China Regional Baseline Emission Factors, 2016 (Exposure Draft). http://qhs.ndrc.gov.cn/gzdt/201704/t20170414_844347.html/. (Accessed 14 April 2017).

Norgate, T., Haque, N., 2010. Energy and greenhouse gas impacts of mining and mineral processing operations. J. Clean. Prod. 18, 266–274. https://doi.org/10.1016/j.jclepro.2009.09.020.

Ogland-Hand, J.D., Bielicki, J.M., Wang, Y.P., Adams, B.M., Buscheck, T.A., Saar, M.O., 2019. The value of bulk energy storage for reducing CO_2 emissions and water requirements from regional electricity systems. Energy Convers. Manag. 181, 674–685. https://doi.org/10.1016/j.enconman.2018.12.019.

O'Sullivan, D., Newman, A., 2015. Optimization-based heuristics for underground mine scheduling. Eur. J. Oper. Res. 241, 248–259. https://doi.org/10.1016/j.ejor.2014.08.020.

Paithankar, A., Chatterjee, S., 2018. Grade and tonnage uncertainty analysis of an african copper deposit using multiple-point geostatistics and sequential Gaussian simulation. Nat. Resour. Res. 27, 419–436. https://doi.org/10.1007/s11053-017-9364-1.

Paricheh, M., Osanloo, M., 2017. A simulation-based framework for estimating probable open-pit mine closure time and cost. J. Clean. Prod. 167, 337–345. https://doi.org/10.1016/j.jclepro.2017.08.202.

Pepekin, V.I., Gubin, S.A., 2007. Heat of explosion of commercial and brisant high explosives. Combust. Explo. Shock 43, 212–218. https://doi.org/10.1007/s10573-007-0029-y.

Peterson, J.S., 2018. Experimental methods to reduce noise generated by haul trucks and LHDs. Noise Control Eng. J. 66, 446–458. https://doi.org/10.3397/1/376638.

Pezzey, J.C.V., Jotzo, F., 2013. Carbon tax needs thresholds to reach its full potential. Nat. Clim. Change 3, 1008–1011. https://doi.org/10.1038/nclimate2054.

Qi, C.C., Ye, L.P., Ma, X.T., Yang, D.L., Hong, J.L., 2017. Life cycle assessment of the hydrometallurgical zinc production chain in China. J. Clean. Prod. 156, 451–458. https://doi.org/10.1016/j.jclepro.2017.04.084.

Rafiee, R., Ataei, M., KhalooKakaie, R., Jalali, S.E., Sereshki, F., Noroozi, M., 2018. Numerical modeling of influence parameters in cavabililty of rock mass in block caving mines. Int. J. Rock Mech. Min. 105, 22–27. https://doi.org/10.1016/j.ijrmms.2018.03.001.

Rahmanpour, M., Osanloo, M., 2017. A decision support system for determination of a sustainable pit limit. J. Clean. Prod. 141, 1249–1258. https://doi.org/10.1016/j.jclepro.2016.09.205.

Rincon, J., Gaydardzhiev, S., Stamenov, L., 2019. Coupling comminution indices and mineralogical features as an approach to a geometallurgical characterization of a copper ore. Miner. Eng. 130, 57–66. https://doi.org/10.1016/j.mineng.2018.10.007.

Rodovalho, E.D., de Tomi, G., 2017. Reducing environmental impacts via improved tyre wear management. J. Clean. Prod. 141, 1419–1427. https://doi.org/10.1016/j.jclepro.2016.09.202.

Roy, M.C., Foote, L., Ciborowski, J.J.H., 2016. Vegetation community composition in wetlands created following oil sand mining in Alberta, Canada. J. Environ. Manag. 172, 18–28. https://doi.org/10.1016/j.jenvman.2016.02.023.

Sepehri, M., Apel, D.B., Hall, R.A., 2017. Prediction of mining-induced surface subsidence and ground movements at a Canadian diamond mine using an elastoplastic finite element model. Int. J. Rock Mech. Min. 100, 73–82. https://doi.org/10.1016/j.ijrmms.2017.10.006.

Shao, S., Liu, J.H., Geng, Y., Miao, Z., Yang, Y.C., 2016. Uncovering driving factors of carbon emissions from China's mining sector. Appl. Energy 166, 220–238. https://doi.org/10.1016/j.apenergy.2016.01.047.

Shi, X.Z., Chen, S.R., 2011. Delay time optimization in blasting operations for mitigating the vibration-effects on final pit walls' stability. Soil Dynam. Earthq. Eng. 31, 1154–1158. https://doi.org/10.1016/j.soildyn.2011.04.004.

Shi, X.Z., Zhou, J., Wu, B.B., Huang, D., Wei, W., 2012. Support vector machines approach to mean particle size of rock fragmentation due to bench blasting prediction. T. Nonferr. Met. Soc. 22, 432–441. https://doi.org/10.1016/S1003-6326(11)61195-3.

Shi, X.Z., Qiu, X.Y., Zhou, J., Chen, X., Fan, Y.Q., Lu, E.W., 2016. Application of Hilbert-Huang transform based delay time identification in optimization of short millisecond blasting. T. Nonferr. Met. Soc. 26, 1965–1974. https://doi.org/10.1016/S1003-6326(16)64310-8.

Sleep, S., Laurenzi, I.J., Bergerson, J.A., Maclean, H.L., 2018. Evaluation of variability in greenhouse gas intensity of Canadian oil sands surface mining and upgrading operations. Environ. Sci. Technol. 52, 11941–11951. https://doi.org/10.1021/acs.est.8b03974.

Stocker, T.F., Qin, D.H., Plattner, G.K., Alexander, L.V., Allen, S.K., Bindoff, N.L., Bréon, F.M., Church, J.A., Cubasch, U., Emori, S., Forster, P., Friedlingstein, P., Gillett, N., Gregory, J.M., Hartmann, D.L., Jansen, E., Kirtman, B., Knutti, R., Kanikicharla, K.K., Lemke, P., Marotzke, J., Delmotte, V.M., Meehl, G.A., Mokhov, I.I., Piao, S.L., Ramaswamy, V., Randall, D., Rhein, M., Rojas, M., Sabine, C., Shindell, D., Talley, L.D., Vaughan, D.G., Xie, S.P., 2013. Technical Summary in Climate Change 2013: the Physical Science Basis. Cambridge University Press, Cambridge, United Kingdom and New York, pp. 33–115. https://doi.org/10.1017/CBO9781107415324.005.

Sui, W.H., Zhang, D.Y., Cui, Z.C., Wu, Z.Y., Zhao, Q.J., 2015. Environmental implications of mitigating overburden failure and subsidences using paste-like backfill mining: a case study. Int. J. Min. Reclam. Environ. 29, 521–543. https://doi.org/10.1080/17480930.2014.969049.

Tyulenev, M., Litvin, O., Cehlar, M., Zhironkin, S., Gasanov, M., 2017. Estimation of hydraulic backhoes productivity for overburden removing at Kuzbass open pits. Acta Montan. Slovaca 22, 296–302.

Villain, L., Alakangas, L., Ohlander, B., 2013. The effects of backfilling and sealing the waste rock on water quality at the Kimheden open-pit mine, northern Sweden. J. Geochem. Explor. 134, 99–110. https://doi.org/10.1016/j.gexplo.2013.08.003.

Wang, M., 2010. Greenhouse Gases, Regulated Emissions, and Energy Use in Transportation (GREET) Model. Center for Transportation Research, Argonne National Laboratory, Argonne, IL version 1.8.d.1.

Wang, X.L., Lin, B.Q., 2017. Factor and fuel substitution in China's iron & steel industry: evidence and policy implications. J. Clean. Prod. 141, 751–759. https://doi.org/10.1016/j.jclepro.2016.09.133.

Wang, P., Dai, H.C., Ren, S.Y., Zhao, D.Q., Masui, T., 2015. Achieving Copenhagen target through carbon emission trading: economic impacts assessment in Guangdong province of China. Energy 79, 212–227. https://doi.org/10.1016/j.energy.2014.11.009.

Whittle, D., Brazil, M., Grossman, P.A., Rubinstein, J.H., Thomas, D.A., 2018. Combined optimisation of an open-pit mine outline and the transition depth to underground mining. Eur. J. Oper. Res. 268, 624–634. https://doi.org/10.1016/j.ejor.2018.02.005.

Woo, K.S., Eberhardt, E., Elmo, D., Stead, D., 2013. Empirical investigation and characterization of surface subsidence related to block cave mining. Int. J. Rock Mech. Min. 61, 31–42. https://doi.org/10.1016/j.ijrmms.2013.01.015.

Xiao, S.S., Li, K.M., Ding, X.H., Liu, T., 2015. Rock mass blastability classification using fuzzy pattern recognition and the combination weight method. Math. Probl Eng. 724619. https://doi.org/10.1155/2015/724619.

Xu, X.C., Gu, X.W., Wang, Q., Liu, J.P., Wang, J., 2014. Ultimate pit optimization with ecological cost for open pit metal mines. T. Nonferr. Met. Soc. 24, 1531–1537. https://doi.org/10.1016/S1003-6326(14)63222-2.

Xu, N.X., Zhang, J.Y., Tian, H., Mei, G., Ge, Q., 2016. Discrete element modeling of strata and surface movement induced by mining under open-pit final slope. Int. J. Rock Mech. Min. 88, 61–76. https://doi.org/10.1016/j.ijrmms.2016.07.006.

Zheng, S., Cheng, K., Wang, J.X., Liao, Q.D., Liu, X.G., Liu, W.W., 2015. Failure analysis of frame crack on a wide-body mining dump truck. Eng. Fail. Anal. 48, 153–165. https://doi.org/10.1016/j.engfailanal.2014.11.013.

Zhou, G.A., Ma, H.H., Shen, Z.W., Chen, P.Y., Yu, Y., 2018. Study on a new cleaner emulsion explosive containing common clay. Propellants, Explos. Pyrotech. 43, 789–798. https://doi.org/10.1002/prep.201700282.